E-ISSN 2586-9027
Homepage : https://tci-thaijo.org/index.php/SciTechAsia Science & Technology Asia
Vol.30 No.3 July - September 2025 Page: [21-29]
*Original research article*

# Microaneurysm Localization in En Face Optical Coherence Tomography Angiography Images

Patsaphon Chandhakanond[1], Yar Zar Tun[1], Seint Lei Naing[1], Misato Tsuji[2], Pakinee Aimmanee[1, *]

[1]*Sirindhorn International Institute of Technology, Thammasat University, Pathum Thani 12120, Thailand*
[2]*Center for Frontier Medical Engineering, Chiba University, Chiba 263-8522, Japan*

Received 14 June 2025; Received in revised form 17 July 2025
Accepted 26 July 2025; Available online 30 September 2025

**ABSTRACT**

A microaneurysm (MA) is a small, round outpouching of a capillary wall in the retina, typically caused by the weakening of the vessel due to diabetic retinopathy. Microaneurysms are generally difficult to detect because they are very small, low-contrast lesions that can be easily obscured by surrounding retinal structures or image noise. This study employed a machine learning method to localize clusters of MAs in en face Optical Coherence Tomography Angiography (OCTA) images. Twelve features were extracted from MA candidates identified through a rule-based method. A support vector machine was then used to filter out non-MA candidates. The density-based spatial clustering of applications with noise (DBSCAN) method was subsequently applied to localize the MA areas. A predicted location is considered correct if it lies within the ground truth MA area. We tested the method on 150 enface OCTA images known to contain MAs and compared it against the rule-based method. The proposed approach significantly improved the average recall of the rule-based method from 48.69% to 59.32%.

**Keywords:** Microaneurysm; Optical coherence tomography angiography; Support vector machine

## 1. Introduction

Diabetic Retinopathy (DR) is a diabetes-related complication and a major cause of adult vision impairment and blindness worldwide. It results from damaged blood vessels of the retina, which is

***Corresponding author:** pakinee@siit.tu.ac.th **doi:** 10.14456/scitechasia.2025.43

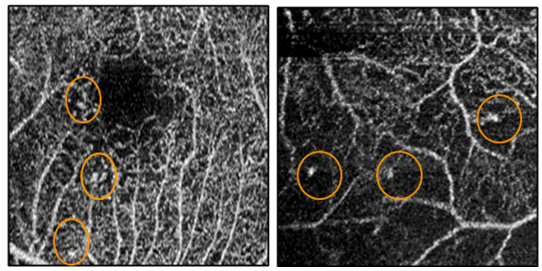

**Fig. 1.** MA lesions detected in en face OCTA images. The bright small white dots are MAs. Yellow boundaries indicate the regions containing MAs.

sensitive tissue at the back of the eye. DR management is critical to prevent vision loss, and the outcome for the patient will be better. One of the earliest visible signs of DR is the presence of microaneurysms (MAs) [1, 2]. Microaneurysms are small outpouchings of capillaries, typically resulting from the weakening of the capillary walls. They are the earliest visible signs of DR. Their presence not only indicates early microvascular damage but also helps in identifying the onset and progression of the disease. Traditional MA detection and DR diagnosis involve manual assessment by ophthalmologists. It is error-ridden, time-consuming, and difficult to implement on mass scales. For this purpose, researchers are using machine learning and artificial intelligence to automate the process and detect MAs and diagnose DR more rapidly.

Technological progress, such as image processing and artificial intelligence, has enhanced the speed and accuracy of medical image analysis. They do not only provide more accurate diagnoses but also allow DR screenings to extend to remote regions with limited resources, thus making it easier to manage diseases and prevent unnecessary blindness.

Identification of MAs, tiny bulges in the blood vessels, is traditionally achieved by fundus photography that provides 2D retinal images. However, Optical Coherence Tomography Angiography (OCTA) has emerged as an even more advanced non-invasive imaging method that provides very high-resolution 3D images of retinal blood flow.

OCTA gives a better image of small blood vessel changes, including capillary issues and MAs, in the different layers of the retina, which makes it very useful for early and accurate detection. Fig. 1 shows a representative MA in en face OCTA images. However, manual analysis of OCTA images is difficult because of data complexity and the faint appearance of MAs, which can resemble other retinal structures like vascular abnormalities, bifurcations of blood vessels, or other lesions. Furthermore, there are other problems, such as noise, low contrast, and artifacts in OCTA images that make MA more difficult to separate from the surrounding structures.

To solve this problem, researchers created automatic systems that use deep learning-based MA detection and machine learning-based image processing for MA localization. These systems aim to increase the accuracy, precision, and efficiency of MA detection and localization in OCTA images and make it easier to be diagnosed by doctors, resulting in an early diagnosis and better patient outcomes.

MAs can appear in both types of images. However, due to the novelty of

OCTA, along with imaging limitations and data scarcity, there are significantly fewer studies on MA localization and segmentation in OCTA compared to fundus images.

Nevertheless, the techniques used for MA localization and segmentation in fundus images are worth reviewing, even though this task is generally easier in fundus images. Therefore, we have also included reviews of the related tasks for fundus images in this paper.

Research studies can be broadly categorized into two primary approaches. The first approach is MA detection using a deep learning model. Deep learning is well-suited for this task because it can automatically learn and identify features from complex, high-resolution images. Convolutional neural networks (CNNs) are effective at spotting small vascular abnormalities like the capillary dilations seen in MAs, even in the presence of noise or image artifacts. Eftekhari et al. [3] developed a two-step CNN-based approach for detecting MAs in fundus images. The first CNN was used to eliminate simple false positives with a cost-effective neural network, while the subsequent CNN is a complex network designed to categorize MA from the remaining candidates. The proposed method obtained a sensitivity value of around 80% in an evaluation with an average of over six false positives per image. Husvogt et al. [4] proposed an ensemble U-Net model for MA segmentation in en face OCTA image of DR patients. To increase segmentation accuracy, the study employed multiple U-Net architectures with varying designs. For the evaluation result, the U-Net model with dice loss and threshold 0.05 achieved the best average F1 per object, around 65%, and the average AUC per pixel, around 70%. Neri et al. [5] suggested a deep learning model to automatically identify MAs of different types in OCT images. The authors trained two deep learning models, YOLO and DETR, on labelled OCT images. The performance of detection and classification was quantified based on the area under the ROC curves. The DETR model achieved the best AUC of 86% for overall MA detection.

Machine learning (ML) has impacted the detection of MAs in retinal images and OCTA significantly and has further driven the domain of medical image processing. The following research has investigated ML methods with retinal images for the detection of MAs in OCTA. Le et al. [6] described and summarized how ML could be used in OCTA, focusing on its role in automated feature extraction and MA detection. They employed eight features related to vessels, such as the size, the area ratio relative to the image size, the locations, tortuosity, and the vessel zone. The accuracy of 82.27% was reported.

The following are studies on MA detection in color fundus images. Long et al. [7] provided a directed local contrast-based method. Their ML-based approach improved feature differentiation, thus enhancing MA detection accuracy and computation time compared to traditional image processing techniques. The proposed method achieves an AUC of the ROC curve of around 87% and 86% on the e-ophtha MA and DIARETDB1 datasets, respectively. Yadav et al. [8] developed a low computational power ML-based method for MA detection from fundus images. The method employed algorithms such as contrast-limited adaptive histogram equalization (CLAHE) [9] for preprocessing, locus segmentation, which is color-based region detection, shape analysis for statistical evaluation, and GLCM for feature extraction. They also evaluated the MA

detection results using several ML models. They reported that the random forest achieved the highest accuracy of 83.33%, respectively. Javidi et al. [10] suggested an MA detection method with discriminative dictionary learning and sparse representation. In their work, a Morlet wavelet algorithm was used to detect all candidates for MA in fundus images. Two discriminative dictionaries were learnt to distinguish MA from non-MA objects and classify them. The proposed method obtains an average sensitivity of 72.01%.

This paper is intended to present a novel method for localizing MAs. The method utilizes image processing and machine learning techniques with different features from existing methods targeting bright, small, and round objects in en face OCTA images for MA localization. This method ensured efficient and precise localization of MAs, resulting in improved diagnostic performance. The remainder of the paper is outlined as follows: Section 2 elaborates on methodology, Section 3 elaborates on the dataset and experiments, Section 4 presents results, and Section 5 provides the conclusion.

## 2. Methodology

The framework of the MA localization task is illustrated in Fig. 2.

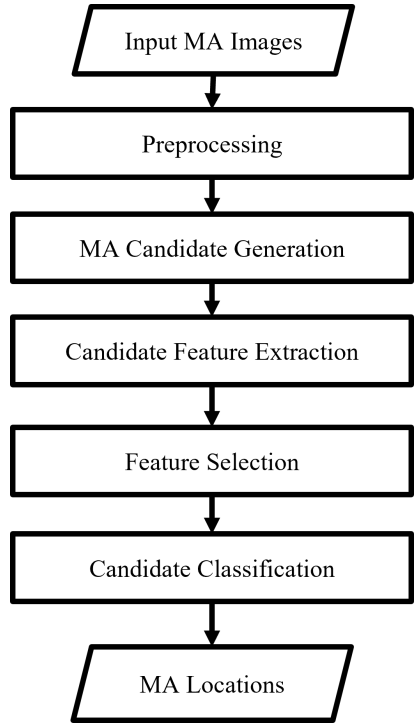


**Fig. 2.** Illustration of the complete preprocessing and machine learning for localizing MAs in en face OCTA images.

### 2.1 Preprocessing

First, the image intensities were normalized to a range of 0 to 1. The image's global contrast enhancement involved scaling the input image's intensity values from the range [0.3, 0.9] to [0, 1]. This re-scaling method ignores parts of the image that are too dark (intensity below 0.3) or too bright (intensity above 0.9) by rendering these regions completely black and white. As a result, this method effectively enhanced the contrast of the region of interest containing MAs, making small, bright dot-like MAs easier to locate. In addition, a 3×3 median filter was applied to preserve the vessel edges and reduce impulsive noise. Finally, the local contrast was improved using CLAHE [9].

### 2.2 MA candidate generation

MA candidates were generated using a traditional rule-based technique. As MAs were typically bright, the pixels with intensity above 0.8 were considered. These pixels formed clusters of various sizes. Because MAs were round and relatively small, we filtered the clusters using the following specific criteria.

Firstly, the area of an object, which is quantified as the count of pixels in the ob-

ject, was used.

Only clusters with an area greater than four pixels but fewer than 30 pixels are considered. This range of areas was derived from the MA areas defined in the work of Wiley et al. [1] and Bakri et al. [2].

Secondly, as MAs are round, circular objects are particularly of our interest. We used eccentricity defined as in Eq. (2.1) to measure circularity.

$$Eccentricity = \sqrt{1 - (\frac{b^2}{a^2})}, \qquad (2.1)$$

where $a$ and $b$ are the lengths of the semi-major and semi-minor axes of an ellipse fitted to the cluster. In this work, an eccentricity of less than or equal to 0.8 is considered based on criteria defined in the study of [11].

Third is the size measured as the radius of a fitted circle to a cluster (Area). Given the Area of the cluster, the ($r$) is mathematically defined as in Eq. (2.2).

$$r = \sqrt{\frac{Area}{\pi}}. \qquad (2.2)$$

In this work, a cluster with a radius less than 3 is focused. The cutoff 3 is selected based on the maximum area of the cluster of 30 specified in the first constraint.

### 2.3 Candidate feature extraction

We extracted twelve features from the MA candidate clusters obtained in the previous step. The features are mainly based on shape and pixel statistical values, listed as follows.

- Area (A): the count of pixels in the object.
- Perimeter (P): the total length of the boundary.
- Diameter: it is calculated as twice the value of the radius defined in Eq. (2.2)
- Eccentricity: This value is mathematically defined in Eq. (2.1).
- Major axis length of the oval fitted to the cluster.
- Minor axis length of the oval fitted to the cluster.
- Circularity: this value is calculated based on the perimeter and area as in Eq. (2.3).

$$Circularity = \frac{4\pi A}{p^2}. \qquad (2.3)$$

- Average pixel intensity (API):

$$API = \frac{1}{N}\sum_{i=1}^{N} I_i, \qquad (2.4)$$

where $I_i$ be the $i^{th}$ intensity of the pixels in the cluster and $N$ is the number of pixels.

The rest of the features are from using a Gray-Level Co-occurrence Matrix (GLCM). They are defined as follows. Let $i$ represent the intensity value of the reference pixel, $j$ represents the intensity value of the neighboring pixel, and $F(i, j)$ is the frequency that a pixel with intensity value $i$ occurs next to a pixel with intensity value $j$, under a given offset (direction and distance).

- Contrast (Ctr): the difference between intensity.

$$Ctr = \sum_{i=1}^{N}\sum_{j=1}^{N}((i-j)^2 F(i,j)). \qquad (2.5)$$

- Energy (Eng), minimum variability in intensity defined in Eq. (2.6).

$$Eng = \sum_{i=1}^{N}\sum_{j=1}^{N} F(i,j)^2. \quad (2.6)$$

- Homogeneity (Hom): uniformity in texture, defined in Eq. (2.7).

$$Hom = \sum_{i=1}^{N}\sum_{j=1}^{N} \frac{F(i,j)}{1+|i-j|}. \quad (2.7)$$

- Entropy (Etp): variability of texture.

$$Etp = -\sum_{i=1}^{N}\sum_{j=1}^{N} (F(i,j)\log_2(F(i,j))). \quad (2.8)$$

### 2.4 Feature selection

To reduce the computational load of the algorithm, Mutual information (MI) [12] was used to filter out non-relevant features from all extracted features. MI verifies each feature's significance by checking its MI score, which indicates how well a feature can predict the class label (MA or not MA).

### 2.5 Candidate classification

We employed machine learning techniques to classify MAs and non-MAs. The Gaussian Support Vector Machine (SVM) classification was optimized via stratified 5-fold cross-validation. The grid search method was used to find the optimal parameters such as kernel scale and penalty, across their suitable ranges. Using these optimal values, the model with the best validation AUC across folds was selected as the best model for each dataset. Then, the model was applied to the whole dataset for the next localization step. While this does not reflect generalization, it offers insight into the upper-bound behavior of the method.

### 2.6 MA localization

After getting the MA's positions, the MA representatives are obtained using the density-based spatial clustering of applications with noise (DBSCAN) method [13]. This method clustered MA blobs based on their spatial proximity. The centroids of the clusters are regarded as the local points of clusters of MAs.

## 3. Dataset and Evaluation

Forty-two en face OCTA images provided by Thammasat University Hospital (TUH) and 108 en face OCTA images from DRAC 2022 [14], which is a public dataset, were used. All images have MA lesions.

Images were 12 mm × 12 mm area scans of superficial retinal layers, centering at the fovea, and were captured at 1024 pixels × 1024 pixels resolution.

The predicted local point was regarded as a true localization if the predicted MA location fell within or on the boundary of the ground truth region. The performance of the MA localization experiment was evaluated using recall (R), precision (P), and F2-score (F2). The formulas are as in Eqs. (2.9)–(2.11).

$$R = \frac{C}{G}, \quad (3.1)$$

$$p = \frac{C}{M}, \quad (3.2)$$

$$F2 = \frac{5P \cdot R}{4P + R}, \quad (3.3)$$

where $C$ is the number of correctly predicted points, $G$ is the number of MA clusters according to ground truths, and $M$ is the number of total predicted points. It is important to note that in this application, as the positive predictive locations are more important than the negative predictive locations, the F2 is used for evaluation rather than the traditional F1-score.

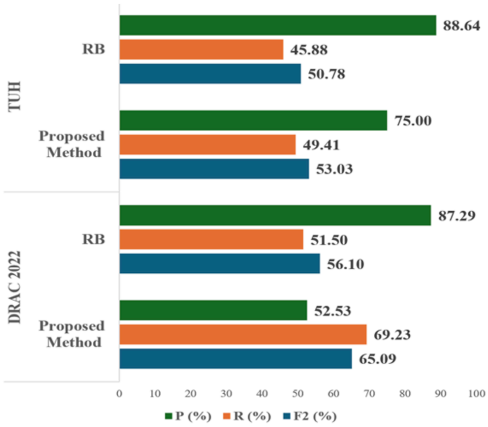


**Fig. 3.** Result comparisons of MA localization of the RB method and the proposed method.

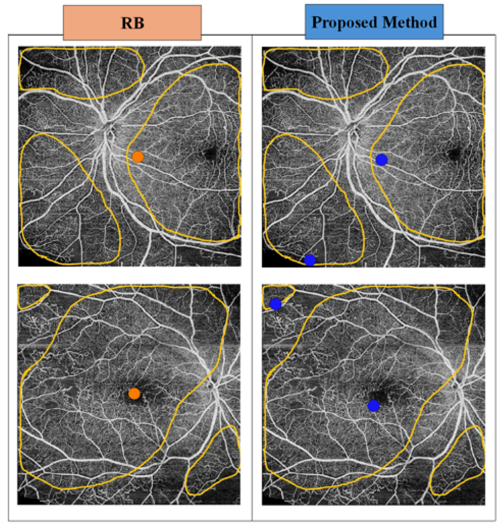


**Fig. 4.** Results comparison of the MA localization of RB and the proposed method.

## 4. Results

We compare our proposed machine learning approach with the rule-based method (RB), as described in Section 2.2. It is important to note that the baseline method consisted of the candidates selected before applying the machine learning models.

As illustrated in Fig. 3, in general, the P values are much higher than the R values for both methods. Although the P values of our proposed method were lower than those of RB, our R values were significantly higher. Consequently, the overall performance F2 of the proposed method was better than that of RB.

The proposed method yields a lower R value than P in the TUH dataset, while in the DRAC22 dataset, P is higher than R. This discrepancy arises because the MA ground truth areas in the TUH dataset are wider than those in the DRAC22 dataset.

This is supported by the average ratio of MA boundary area to total image area, which is 0.46 in the TUH dataset compared to only 0.41 in the DRAC22 dataset. The wider areas in the TUH dataset make it more challenging for the proposed method to detect all relevant areas, resulting in a lower R value. Conversely, the higher P value indicates a greater likelihood that the predictions were accurate. In comparison, the rule-based method exhibits much higher precision because the detected MAs are more widely spread compared to those identified by the proposed method, increasing the likelihood of overlapping with the ground truth region. However, the broader predicted area for MAs results in significantly more incorrect detections than the proposed method, leading to lower R values. This trend is particularly evident in the DRAC2022 dataset, where the ground truth areas are less dispersed.

The MA localization result from trained images is illustrated in Fig. 4.

As seen in Fig. 4, the RB method gave correct localization on some lesions. The proposed method, which uses ML methods, improves the localization recall, it can pinpoint more locations of MAs.

However, due to the difficult nature of the problem, more false localizations

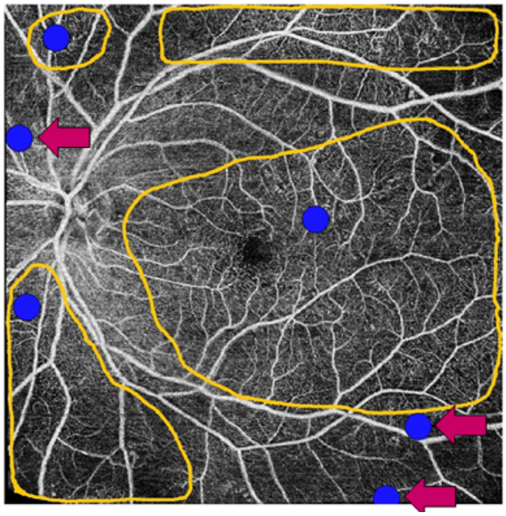

**Fig. 5.** Illustration of the cases for falsely predicted locations (red arrows) of the proposed method.

were also seen in some cases using the proposed method. Fig. 5 illustrates a case where false predictions were seen as a drawback when SVM is involved.

## 5. Conclusion

Microaneurysms (MAs) in en face OCTA images are vital for diagnosing early diabetic retinopathy (DR), yet manual detection is challenging due to image complexity, subtle MA presentation, noise, and low contrast. We employed image processing combined with a Gaussian SVM model and compared it with a rule-based method for MA localization. The proposed model, which utilizes SVM, gives an average recall of 59.32%, which is 10.63% better than the rule-based method. Although the rule-based method had higher precision, it tended to miss true cases. Our SVM-based technique consistently localized MAs with better recall and F2 score across datasets, indicating enhanced sensitivity to positive instances. These findings underscore the value of integrating thresholding with SVM for more balanced classification. Some lesions remained undetected, prompting future work exploring adaptive thresholding, deep learning models, and improved feature selection to boost robustness and sensitivity.

## Acknowledgements

We sincerely thank Thailand Science Research and Innovation (Grant number TUFF 48/2568) and the center of excellence in biomedical engineering of Thammasat University for financial support of this research. Mr. Chandhakanond was grateful to the Sirindhorn International Institute of Technology, Thammasat University for awarding him the Excellent Thai Scholarship for his studies.

## References

[1] Wiley HE, Ferris FL. Nonproliferative diabetic retinopathy and diabetic macular edema. In: Ryan SJ, editor. Retina. London: Elsevier; 2013. p. 940–68.

[2] Bakri SJ, Kaiser PK. Diabetic retinopathy. In: Spaide RF, Costa RA, editors. Retinal imaging. 1st ed. Philadelphia: Saunders Elsevier; 2006. p. 233–40.

[3] Eftekhari N, Pourreza HR, Masoudi M, Ghiasi-Shirazi K, Saeedi E. Microaneurysm detection in fundus images using a two-step convolutional neural network. Biomed Eng Online. 2019;18:67.

[4] Husvogt L, Yaghy A, Camacho A, Lam A, Schottenhamml J, Ploner SB, et al. Ensembling U-Nets for microaneurysm segmentation in optical coherence tomography angiography in patients with diabetic retinopathy. Sci Rep. 2024;14:21520.

[5] Neri G, Sharma S, Ghezzo B, Novarese C, Olivieri C, Tibaldi D, et al. Deep learning model for automatic detection of different types of microaneurysms in diabetic retinopathy. Eye (Lond). 2025;39:570–7.

[6] Le D, Son T, Yao X. Machine learning in optical coherence tomography angiography. Exp Biol Med (Maywood). 2021;246(20):2170–83.

[7] Long S, Chen J, Hu A. Microaneurysms detection in color fundus images using machine learning based on directional local contrast. Biomed Eng Online. 2020;19:21.

[8] Yadav D, Karn AK, Giddalur A, Dhiman A, Sharma S, Muskan, Yadav AK. Microaneurysm detection using color locus detection method. Measurement. 2021;176:109084.

[9] Zuiderveld K. Contrast limited adaptive histogram equalization. In: Heckbert P, editor. Graphics gems IV. San Diego: Academic Press; 1994. p. 474–85.

[10] Javidi M, Pourreza HR, Harati A. Vessel segmentation and microaneurysm detection using discriminative dictionary learning and sparse representation. Comput Methods Programs Biomed. 2017;139:93–108.

[11] Orbital motion: eccentricity. Columbus (OH): The Ohio State University; [cited 2025 Jun 12]. Available from: https://www.asc.ohio-state.edu/orban.14/stemcoding/eccentricity/eccentricity.html

[12] Suleiman M, Labadin J. Improved feature selection based on mutual information for regression tasks (IFSMIR). J IT Asia. 2016;6.

[13] Birant D, Kut A. ST-DBSCAN: An algorithm for clustering spatial–temporal data. Data Knowl Eng. 2007;60:208–21.

[14] Qian B, Xiong Y, Lu H, Ding Y, Lin Y, Liang J, et al. Drac 2022: A public benchmark for diabetic retinopathy analysis on ultra-wide optical coherence tomography angiography images. Patterns. 2024;5(3):100929.